J|A|C|S
ARTICLES
Published on Web 01/31/2007

Donor−Acceptor Biradicals as Ground State Analogues of Photoinduced Charge Separated States

Martin L. Kirk,*,† David A. Shultz,*,‡ Ezra C. Depperman,† and Candice L. Brannen‡

Contribution from the Department of Chemistry, The University of New Mexico, MSC03 2060, 1 University of New Mexico, Albuquerque, New Mexico 87131-0001, and Department of Chemistry, North Carolina State University, Raleigh, North Carolina 27695-8204

Received July 26, 2006; E-mail: mkirk@unm.edu; david_shultz@ncsu.edu

Abstract: A Valence Bond Configuration Interaction (VBCI) model is used to relate the intraligand magnetic exchange interaction (J) to the electronic coupling matrix element (H_{AB}) in $Tp^{Cum,Me}Zn$(SQNN), a compound that possesses a Donor−Acceptor (D−A) *S*emi*Q*uinone-*N*itronyl*N*itroxide (SQNN) biradical ligand. Within this framework, an SQ → NN charge transfer state mixes with the ground state and stabilizes the spin triplet ($S = 1$). This charge-transfer transition is observed spectroscopically and probed using resonance Raman spectroscopy. In addition, the temperature-dependent electronic absorption spectrum of the Ni(II) complex, $Tp^{Cum,Me}$Ni(SQNN), has been studied. Exchange coupling between the $S = 1$ Ni(II) ion and $S = 1$ SQNN provides a mechanism for observing the formally spin-forbidden, ligand-based ^{3}GC → ^{1}CTC transition. This provides a means of determining U, the mean GC → CTC energy, and a one-center exchange integral, K_0. The experimental determination of J, U, and K_0 permits facile calculation of H_{AB}, and we show that this methodology can be extended to determine the electronic coupling matrix element in related SQ−Bridge−NN molecules. As magnetic susceptibility measurements are easily acquired in the solid state, H_{AB} may be effectively determined for single molecules in a known geometry, provided a crystal structure exists for the biradical complex. Thus, SQ−Bridge−NN molecules possess considerable potential for probing both geometric and electronic structure contributions to the magnitude of the electronic coupling matrix element associated with a given bridge fragment.

Introduction

Numerous experimental and theoretical studies have been undertaken that evaluate the contribution of a molecular bridge (B) fragment in facilitating photoinduced electron transfer (PET) between donor (D) and acceptor (A) moieties. Along these lines, various models have been developed to understand the rates of adiabatic and nonadiabatic electron transfer as a function of the thermodynamic driving force and the geometry and nature of the bridge.[1−16] Photoexcitation of the D fragment in a D−B−A system initially results in an D*−B−A excited state that can undergo electron transfer to form a D^+−B−A^- charge-separated state. These D^+−B−A^- charge-separated states are typically formed in solution and probed by temporal spectroscopies such as transient and time-resolved absorption and Raman. Three fundamental mechanisms are responsible for nonresonant charge-transfer processes in molecular systems.[17] The superexchange mechanism involves electron (e^-) or hole (h^+) transfer via the bridge and does not involve discrete redox changes in the bridge. The other mechanisms are incoherent e^-/h^+ tunneling and thermally activated hopping, the latter of which involves oxidation or reduction of the bridge. Importantly, key excited-state contributions to the nature of the D^+−B−A^- charge-separated configuration have not been explored in detail, since in the traditional PET experiment direct probing of the D^+−B−A^- state necessitates a two-photon process. Furthermore

† The University of New Mexico.
‡ North Carolina State University.

(1) Barbara, P. F.; Meyer, T. J.; Ratner, M. A. *J. Phys. Chem.* **1996**, *100*, 13148−13168.
(2) Marcus, R. A. *Chem. Phys. Lett.* **1987**, *133*, 471−477.
(3) Gray, H. B.; Walther, R.; Ellis, J. Electron Transfer. In *Bioinorganic Chemistry*; Bertini, I., Gray, H. B., Lippard, S. J., Valentine, J. S., Eds. University Science Books: Sausalito, CA, 1994; pp 315−364.
(4) Nakamoto, T.; Yoshida, M.; Kitagawa, S.; Katada, M.; Endo, K.; Sano, H. *Polyhedron* **1996**, *15*, 2131−2139.
(5) Wall, M. H.; Basu, P.; Buranda, T.; Wicks, B. S.; Findsen, E. W.; Ondrias, M.; Enemark, J. H.; Kirk, M. L. *Inorg. Chem.* **1997**, *36*, 5676−5677.
(6) Sekiguchi, S.; Kobori, Y.; Akiyama, K.; Tero-Kubota, S. *J. Am. Chem. Soc.* **1998**, *120*, 1325−1326.
(7) Bleuzen, A.; Lomenech, C.; Dolbecq, A.; Villain, F.; Goujon, A.; Roubeau, O.; Nogues, M.; Varret, F.; Baudelet, F.; Dartyge, E.; Giorgetti, C.; Gallet, J. J.; Moulin, C. C. D.; Verdaguer, M. *Mol. Cryst. Liq. Cryst. Sci. Technol., Sect. A* **1999**, *334*, 965−974.
(8) Nelsen, S. F.; Ismagilov, R. F.; Gentile, K. E.; Powell, D. R. *J. Am. Chem. Soc.* **1999**, *121*, 7108−7114.
(9) Kuciauskas, D.; Liddell, P.; Lin, S.; Stone, S.; Moore, A.; Moore, T.; Gust, D. *J. Phys. Chem. B* **2000**, *104*, 4307−4321.
(10) Lewis, F.; Wu, T.; Liu, X.; Letsinger, R.; Greenfield, S.; Miller, S.; Wasielewski, M. *J. Am. Chem. Soc.* **2000**, *122*, 2889−2902.
(11) Miller, S.; Lukas, A.; Marsh, E.; Bushard, P.; Wasielewski, M. *J. Am. Chem. Soc.* **2000**, *122*, 7802−7810.
(12) Sato, O.; Hayami, S.; Gu, Z.; Seki, K.; Nakajima, R.; Fujishima, A. *Chem. Lett.* **2001**, 874−875.
(13) Davis, W. B.; Ratner, M. A.; Wasielewski, M. R. *Chem. Phys.* **2002**, *281*, 333−346.
(14) Tachikawa, T.; Kobori, Y.; Akiyama, K.; Katsuki, A.; Usui, Y.; Steiner, U. E.; Tero-Kubota, S. *Mol. Phys.* **2002**, *100*, 1413−1420.
(15) Lukas, A. S.; Bushard, P. J.; Weiss, E. A.; Wasielewski, M. R. *J. Am. Chem. Soc.* **2003**, *125*, 3921−3930.
(16) Goldsmith, R. H.; Sinks, L. E.; Kelley, R. F.; Betzen, L. J.; Liu, W. H.; Weiss, E. A.; Ratner, M. A.; Wasielewski, M. R. *Proc. Natl. Acad. Sci. U.S.A.* **2005**, *102*, 3540.
(17) Weiss, E. A.; Tauber, M. J.; Kelley, R. F.; Ahrens, M. J.; Ratner, M. A.; Wasielewski, M. R. *J. Am. Chem. Soc.* **2005**, *127*, 11842.

10.1021/ja065384t CCC: $37.00

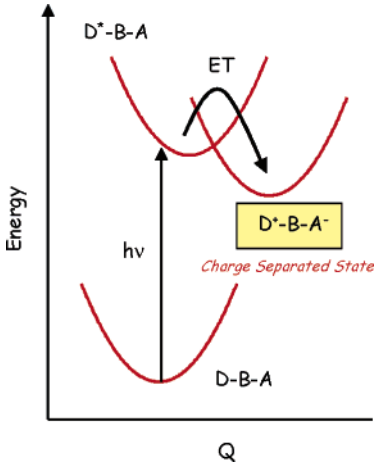

Figure 1. Potential energy diagram for PET showing the charge separated state as a D−B−A biradical.

direct measurement of the electronic coupling matrix element (H_{AB}) is generally not possible in D−B−A systems because the electron-transfer rate is very dependent on intramolecular and solvent reorganization energies.[18−20] Stable D−B−A biradicals are effectively *ground state analogues* of the charge separated state (Figure 1). As such, detailed electronic studies of stable ground state donor−acceptor biradical systems provide a convenient platform for evaluating key electronic structure contributions to the magnitude of H_{AB}, and the contributions of the bridge fragment through detailed spectroscopic and magnetic studies of analogues for the D^+-B^--A excited configuration that figures prominently in superexchange and hopping mechanisms.

Regarding D−B−A systems, electronic interactions between covalently linked organic radicals can also be quite strong owing to direct exchange between the individual spin centers.[21−24] Specifically, covalently bound nondisjoint donor−acceptor biradicals[25] that constitute a D−A pair can possess extremely strong intramolecular *ferromagnetic* interactions and display potential as key organic linker components in the construction of high-spin supramolecules. Recently we have applied a valence bond configuration interaction (VBCI) model in order to provide a framework for understanding the electronic origin of the strong ferromagnetic coupling in the semiquinone-nitronylnitroxide (SQNN) D−A biradical series, $Tp^{Cum,Me}M$(SQNN) ($Tp^{Cum,M}$ = hydro-tris(3-cumenyl-5-methylpyrazolyl)borate; M = transition metal ion, Scheme 1), which provides key design criteria for the synthesis of new *high-spin* biradicals.[21−24] This model owes much to the early VB work of Heitler and London,[26] based on Heisenberg's resonance approach,[27] detailing the origin of the chemical bond in H_2. The VBCI model differs from the more common molecular orbital model in that it provides a state, as opposed to orbital, description of the system. Thus, the VBCI approach is more amenable to spectroscopic investigations since electronic transitions occur between states. In this model, covalency is manifested by configurational mixing of charge-transfer excited states into the ground state via the electronic coupling matrix element, H_{AB}. Since the biradical ligand exchange interaction in $Tp^{Cum,Me}M$(SQNN) is so strong, the donor and acceptor radicals may be covalently linked by various spacer (bridge) groups and still retain their strong ferromagnetic coupling. Expressions have been developed that relate the measured exchange coupling parameter, J, with H_{AB}, which describes the transfer of an electron from donor to acceptor.[28−35] Thus, our D−B−A complexes are excellent systems for the study of orbital and pathway dependent electronic coupling contributions to electron transfer through the bridge fragment. As magnetic susceptibility measurements are easily acquired in the solid state, H_{AB} may be effectively determined *for single molecules in a known geometry*, provided a crystal structure exists for the biradical complex. In summary, D−B−A biradicals possess considerable potential for probing electronic structure contributions to the design of molecular electron transport conduits, including technologies that exploit magnetic bridge fragments and those that promote unidirectional electron flow.[16,17,34,36−44]

Experimental Section

All compounds were synthesized as previously described.[22]

Electronic Absorption Spectroscopy. Electronic absorption spectra were collected on a Hitachi U-3501 UV−vis−NIR spectrophotometer capable of scanning a wavelength region between 185 and 3200 nm using a double-beam configuration at 2.0 nm resolution. The instrument wavelength was calibrated with reference to the 656.10 nm deuterium line. Background spectra were collected to correct for residual absorption due to the solvent or mulling agent and automatically subtracted from the sample spectrum by the Hitachi Grams software. Low temperature (~10 K) spectra were collected using a Janis STVP-100 continuous flow cryostat mounted in a custom designed cradle assembly, and the sample temperature was monitored with a Lakeshore silicon diode (PT-470) and regulated by a combination of helium flow and dual heater assemblies. Solution spectra were collected in 1.0 mm path length spectrosil quartz masked cells (Starna). Solution samples were

(18) Forbes, M. D. E.; Ball, J. D.; Avdievich, N. I. *J. Am. Chem. Soc.* **1996**, *118*, 4707−4708.
(19) Forbes, M. D. E. *J. Phys. Chem.* **1993**, *97*, 3396−3400.
(20) Forbes, M. D. E. *J. Phys. Chem.* **1993**, *97*, 3390−3395.
(21) Depperman, E.; Bodnar, S. H.; Vostrikova, K. E.; Shultz, D. A.; Kirk, M. L. *J. Am. Chem. Soc.* **2001**, *123*, 3133−3134.
(22) Shultz, D.; Vostrikova, K.; Bodnar, S.; Koo, H.; Whangbo, M.; Kirk, M.; Depperman, E.; Kampf, J. *J. Am. Chem. Soc.* **2003**, *125*, 1607−1617.
(23) Kirk, M. L.; Shultz, D. A.; Depperman, E. C. *Polyhedron* **2005**, *24*, 2880.
(24) Shultz, D. A.; Kumar, R. K.; Bin-Salamon, S.; Kirk, M. L. *Polyhedron* **2005**, *24*, 2876.
(25) Borden, W. T. *Mol. Cryst. Liq. Cryst.* **1993**, *232*, 195.
(26) Heitler, W.; London, F. *Z. Phys.* **1927**, *44*, 455.
(27) Heisenberg, W. *Z. Phys.* **1926**, *38*, 411.
(28) Anderson, P. W.; Hasegawa, H. *Phys. Rev.* **1955**, *100*, 675−681.
(29) Hatfield, W. E. Chapter 7. Properties of Condensed Compounds (Compounds with Spin Exchange). In *Theory and Applications of Molecular Paramagnetism*; Boudreaux, E. A., Mulay, L. N., Eds. Wiley-Interscience: New York, 1976; pp 381−385.
(30) Brunold, T. C.; Gamelin, D. R.; Solomon, E. I. *J. Am. Chem. Soc.* **2000**, *122*, 8511−8523.
(31) Weiss, E. A.; Tauber, M. J.; Ratner, M. A.; Wasielewski, M. R. *J. Am. Chem. Soc.* **2005**, *127*, 6052.
(32) Weiss, E. A.; Wasielewski, M. R.; Ratner, M. A. *J. Chem. Phys.* **2005**, *123*, 064504.
(33) Weiss, E. A.; Ahrens, M. J.; Sinks, L. E.; Ratner, M. A.; Wasielewski, M. R. *J. Am. Chem. Soc.* **2004**, *126*, 9510.
(34) Weiss, E. A.; Ahrens, M. J.; Sinks, L. E.; Gusev, A. V.; Ratner, M. A.; Wasielewski, M. R. *J. Am. Chem. Soc.* **2004**, *126*, 5577.
(35) Blondin, G.; Girerd, J. J. *Chem. Rev.* **1990**, *90*, 1359−1376.
(36) Ke, S. H.; Baranger, H. U.; Yang, W. T. *Phys. Rev. B* **2005**, *71*, 113401.
(37) Liu, R.; Ke, S. H.; Baranger, H. U.; Yang, W. T. *J. Chem. Phys.* **2005**, *122*, 044703.
(38) Davis, W. B.; Svec, W. A.; Ratner, M. A.; Wasielewski, M. R. *Nature* **1998**, *396*, 60−63.
(39) Stabel, A.; Herwig, P.; Mullen, K.; Rabe, J. P. *Angew. Chem., Int. Ed. Engl.* **1995**, *34*, 1609−1611.
(40) Hutchison, G. R.; Ratner, M. A.; Marks, T. J. *J. Am. Chem. Soc.* **2005**, *127*, 2339.
(41) Stokbro, K.; Taylor, J.; Brandbyge, M. *J. Am. Chem. Soc.* **2003**, *125*, 3674−3675.
(42) Metzger, R. *Mater. Sci. Eng.* **1995**, C3, 277−285.
(43) Joachim, C.; Ratner, M. A. *Proc. Natl. Acad. Sci. U.S.A.* **2005**, *102*, 8801.
(44) Aviram, A.; Ratner, M. A. *Chem. Phys. Lett.* **1974**, *29*, 277.

Scheme 1. Molecules $Tp^{Cum,Me}M(SQNN)$ and ArNN

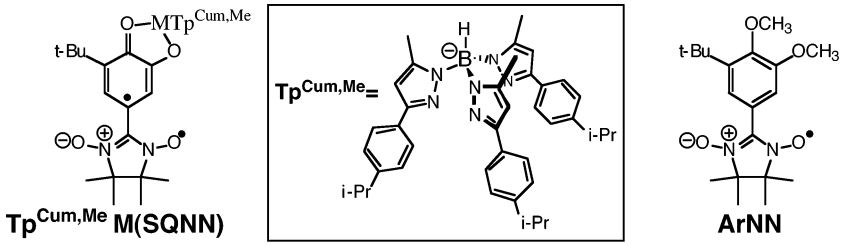

prepared in dichloromethane except for $Tp^{Cum,Me}Cu(SQNN)$ and $Tp^{Cum,Me}Zn(SQNN)$ and ArNN (Scheme 1) which were dissolved in methylcyclohexane. Solid-solution spectra were collected on thin polystyrene polymer films prepared by evaporation of the saturated polystyrene solutions dispersed on glass. Gaussian resolution of spectral bands and corrections for light scattering were accomplished with the Grams 386 software package.

Resonance Raman Spectroscopy. Coherent Innova 70-5 Ar^+ ion (457.9−528.7 nm) and Coherent Innova 300C Kr^+ ion (406.7−676.4 nm) lasers were used as the excitation sources. The scattered radiation was dispersed onto a liquid N_2 cooled 1" Spex Spectrum One CCD detector using a Spex 1877E triple grating monochromator equipped with 600, 1200, and 1800 gr/mm holographic gratings at the spectrographic stage. The laser power at the sample was kept between 40 and 100 mW to prevent thermal degradation or photodegradation of the sample. Solid samples were prepared as finely ground powders and dispersed into finely ground $NaNO_3$ until the mixture was homogeneous. Solution samples were prepared in CH_2Cl_2. The prepared samples were then sealed in an NMR tube with a rubber septum and Parafilm. Room-temperature spectra were obtained with the sample tube placed in a modified NMR sample holder/spinner and collected using a 135° backscattering geometry.

Electronic Structure Calculations. Electronic structure and vibrational frequency calculations were performed at the density functional level of theory using the Gaussian 03W software package. All calculations employed the B3LYP hybrid functional and used a 6-311G++ basis set, including diffuse and polarizability functions for all atoms. Input files were prepared using the molecule builder function in the Gaussview software package.

Results and Discussion

Spectroscopic Studies. An overlay of the room-temperature electronic absorption spectra for $Tp^{Cum,Me}Cu(SQNN)$ and $Tp^{Cum,Me}Zn(SQNN)$ is presented in Figure 2. It is apparent that the absorption spectrum of $Tp^{Cum,Me}Zn(SQNN)$ is only slightly blue-shifted from that of the Cu analogue, indicating that the nature of the divalent metal plays only a minor role in affecting the electronic absorption spectra.[23] Otherwise, the spectra of these, and other $Tp^{Cum,Me}M(SQNN)$ compounds, are virtually identical. This indicates that the observed spectral features dominantly derive from SQNN intraligand-based transitions with no discernible bands being ligand field, LMCT, or MLCT in nature. For $Tp^{Cum,Me}Cu(SQNN)$, a broad low-energy absorption feature is found in the 10 000−15 000 cm^{-1} region ($\epsilon \approx 625$ M^{-1} cm^{-1}), assignable as an SQ $n \rightarrow \pi^*$ transition by analogy with other SQ-based chromophores. Similarly, the ~18 000 cm^{-1} ($\epsilon \approx 1875$ M^{-1} cm^{-1}) band is assigned as an NN-based $n \rightarrow \pi^*$ transition based on the spectroscopic similarity with the aryl-nitronylnitroxide, ArNN (Scheme 1). Additional, higher energy transitions are observed at 24 500 cm^{-1} ($\epsilon \approx 13\,500$ M^{-1} cm^{-1}) and 29 000 cm^{-1} ($\epsilon \approx 13\,000$ M^{-1} cm^{-1}), with a shoulder on the latter at 30 300 cm^{-1} ($\epsilon \approx 10\,200$ M^{-1} cm^{-1}). The 29 000 cm^{-1} band is assigned as a NN-based $\pi \rightarrow \pi^*$ transition, based upon the spectrum of ArNN. Interestingly, the ~24 500 cm^{-1} band is not present in absorption spectra of either $Tp^{Cum,Me}Zn(SQ)$[45] or the aryl nitronylnitroxide, ArNN, which possess the SQ and NN constituent chromophores of the SQNN ligand (Scheme 1), indicating that this transition is intrinsic to the SQNN chromophore (Figure 3).

Aside from the uniqueness of the 25 000 cm^{-1} transition to SQNN, additional support for the SQ-$\pi \rightarrow$ NN-π^* assignment is derived from resonance Raman (rR) spectroscopic studies on $Tp^{Cum,Me}Cu(SQNN)$. Resonance Raman spectra collected at 413.7 nm and 488 nm for $Tp^{Cum,Me}Cu(SQNN)$ are shown in Figure 4. More than 20 vibration bands are found to be resonantly enhanced when pumping into the 24 500 cm^{-1} (408 nm) absorption band, and at least 11 vibrational bands are observed in the 1200−1600 cm^{-1} region where the dominant in-plane SQNN ligand stretching vibrations are anticipated to occur. Vibrational frequencies and normal mode descriptions have been obtained from DFT frequency calculations, and the results for the in-plane stretching region are compared with the experimental data and presented in Table 1. The large number of observed in-plane vibrations, coupled with the fact that the vibrations are delocalized over the entire SQNN chromophore, is fully consistent with an assignment of the 24 500 cm^{-1} band as an intraligand SQ $\rightarrow$ NN charge transfer, underscoring the donor−acceptor nature of the SQNN ligand. Additionally, rR excitation profiles have been constructed for the 1407 cm^{-1} and 1482 cm^{-1} modes, which possess in-plane vibrational motions in both the NN[46,47] and SQ[48] fragments (Figure 5). The resonance Raman excitation profiles are consistent with the intraligand charge-transfer nature of the 24 500 cm^{-1} band in $Tp^{Cum,Me}M(SQNN)$, as vibrations common to the coupled SQNN chromophore are resonantly enhanced. In summary, an intense intraligand SQ-$\pi \rightarrow$ NN-π^* CT transition is observed in $Tp^{Cum,Me}M(SQNN)$ that is unique to this composite chromophore.

Frontier Molecular Orbital Description of Biradicial SQNN and Evaluation of the Singlet−Triplet Gap. Spin unrestricted density functional theory calculations have been performed on NN, SQ, and SQNN in order to gain additional insight into the electronic structure of the SQNN biradical ligand and the electronic origin of the large ferromagnetic exchange coupling in the SQNN biradical, which leads to the high spin $S = 1$ ground state.[22,49] The highest occupied NN orbital (Figure 6), 43α, is a π-type molecular orbital comprised of p_z atomic

(45) Ruf, M.; Noll, B. C.; Groner, M. D.; Yee, G. T.; Pierpont, C. G. *Inorg. Chem.* **1997**, *36*, 4860−4865.
(46) Xiao, C.; Feng, K.; Mo, Y.; Meng, Q.; Zhang, M.; Wan, M.; Zhao, J. *Chem. Phys.* **1998**, *237*, 73−79.
(47) Mo, Y.-J.; Li, Y.-C.; Zhao, J.-G.; Fen, K.-A.; Xiao, C.-Y.; Wan, M.-X. *J. Magn. Magn. Mater.* **2000**, *213*, 278−280.
(48) Lynch, M. W.; Valentine, M.; Hendrickson, D. N. *J. Am. Chem. Soc.* **1982**, *104*, 6982.

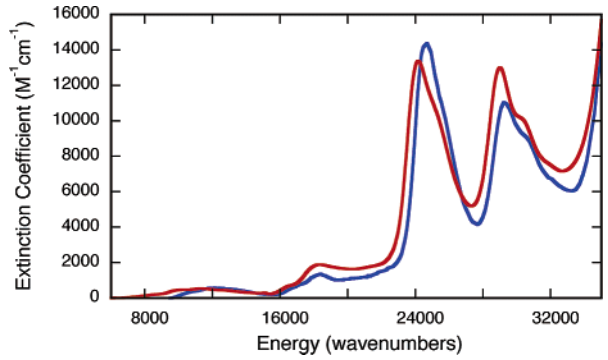

Figure 2. Room-temperature electronic absorption spectra of $Tp^{Cum,Me}$-Cu(SQNN) (red) and $Tp^{Cum,Me}$Zn(SQNN) (blue).

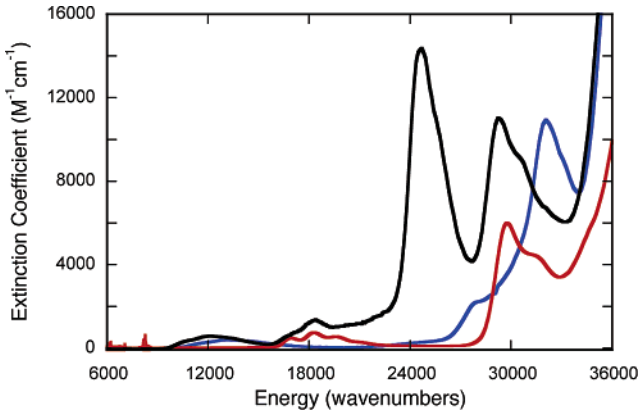

Figure 3. Room-temperature electronic absorption spectra of $Tp^{Cum,Me}$-Zn(SQNN) (black), ArNN (red), and $Tp^{Cum,Me}$Zn(SQ) (blue). Note: the spectrum of ArNN has been blue-shifted by 2000 cm^{-1} for comparative purposes.

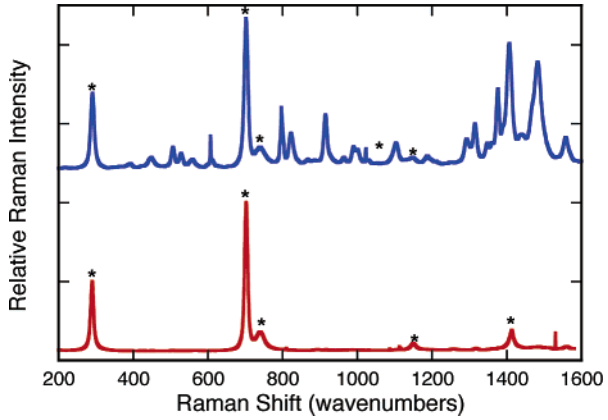

Figure 4. Room-temperature resonance Raman spectra of $Tp^{Cum,Me}$Cu-(SQNN) at 488 nm (red) and 413.7 nm (blue). Solvent modes are marked with an asterisk.

orbital functions localized on the N and O atoms. Importantly, there is no coefficient on the central carbon in the highest occupied NN 43α orbital, which bridges to the SQ fragment in SQNN. The situation regarding the NN fragment is analogous to that of the pentadienyl dianion radical, the SOMO of which has a node at the central carbon. The highest occupied majority spin orbital for the SQ radical is 33α, a π-type molecular orbital delocalized over all ring C atoms and the semiquinone O atoms and is depicted in Figure 6. Thus, the SQNN spin bearing orbitals which are analogous to NN 43α and SQ 33α should

(49) Kirk, M. L.; Shultz, D. A.; Depperman, E. *Polym. J.* **2004**.

Table 1. Experimental Raman Frequencies, Calculated Vibrational Frequencies, and Mode Assignments for $Tp^{Cum,Me}$Cu(SQNN)

experimental $Tp^{Cum,Me}$Cu(SQNN) rR frequency (cm^{-1})	calculated SQNN rR frequency (cm^{-1})	assignment (dominant in-plane motion)
1000		SQ $C_\beta-C_\gamma$ stretch
1026	1025	NN $C_\alpha-N$ stretch
1106		SQ $C_\alpha-C_\beta$ stretch
1148	1147	NN $N-C_\alpha-N$ bend
1190	1185	NN $N-C_\beta$ stretch
1291	1291	SQ $C_\beta-C_\gamma$ stretch
		NN $N-C_\beta-N$ wag
1315	1299	SQ C−O stretch
		NN ring breathing
1348	1352	SQ C−O stretch
		NN N−O stretch
1375	1374	SQ C−O stretch
		NN $C_\alpha-N-C_\beta$ bend
1407	1401	SQ $C_\gamma-C_\delta$ stretch
		NN $C_\alpha-N-C_\beta$ bend
1440	1423	SQ C−O stretch
		NN ring breathing
	1446	SQ C−O stretch
		NN ring breathing
1482	1460	SQ C−O stretch
		NN ring breathing
	1490	SQ C−O s stretch
		SQ $C_\alpha-C_\beta$ stretch
		NN $C_\alpha-N$ stretch
1557	1553	SQ C−O stretch
		NN ring breathing

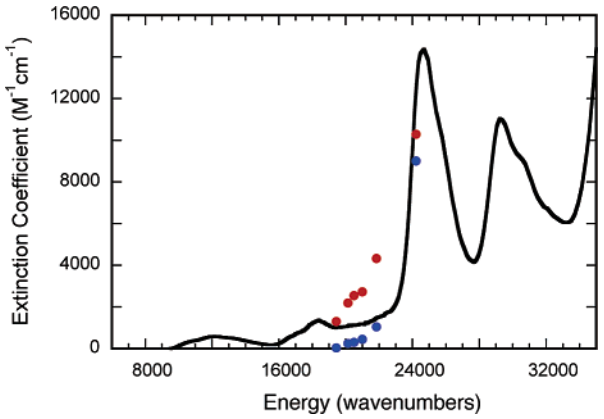

Figure 5. Resonance Raman excitation profiles of the 1407 cm^{-1} (closed red circles) and 1482 cm^{-1} (closed blue circles) modes of $Tp^{Cum,Me}$Cu-(SQNN).

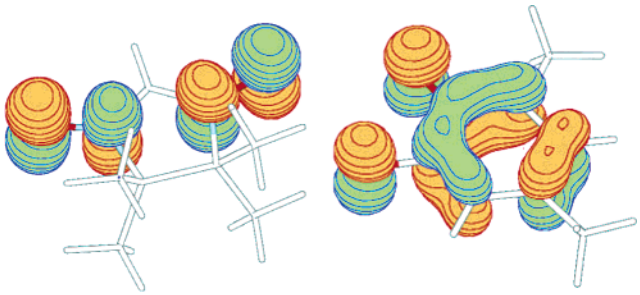

Figure 6. SOMO wavefunctions for NN (left) and SQ (right).

be responsible for determining the sign and magnitude of the magnetic exchange parameter, 2*J*, which defines the nature of the singlet−triplet gap in $Tp^{Cum,Me}$Zn(SQNN).

Spin-restricted DFT calculations on the SQNN biradical ligand are fully consistent with the computational results for the constituent SQ and NN chromophores and lead to the

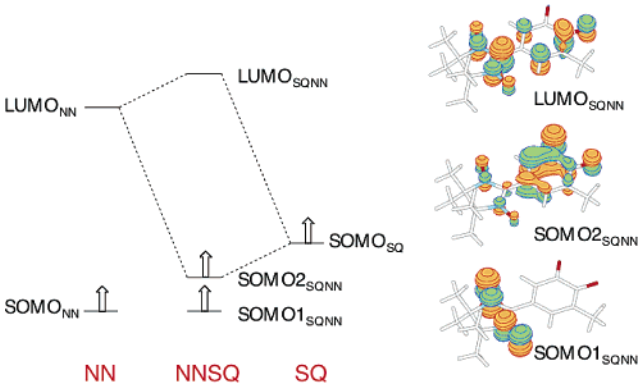

Figure 7. Molecular orbital mixing diagram (left) and frontier π-MO wavefunctions for SQNN (right).

simplified molecular orbital diagram and valence molecular orbitals shown in Figure 7. Interestingly, the nature of the constituent SQ and NN SOMO wavefunctions precludes any direct exchange interaction between them. The key observation here is that the central carbon atom on the NN SOMO, which is directly connected to the SQ ring C_α carbon, possesses no p_z atomic orbital coefficient in the LCAO expansion of the NN SOMO wavefunction. As such, the $\langle SOMO_{NN}|SOMO_{SQ}\rangle$ overlap integral in SQNN is anticipated to be zero, requiring one to proceed beyond the active electron approximation and include virtual orbitals (i.e., $LUMO_{NN}$) in the analysis of the magnetic exchange. In contrast to the NN SOMO, the NN LUMO wavefunction possesses a dominant contribution from the central carbon atom, allowing for a nonzero $\langle LUMO_{NN}|SOMO_{SQ}\rangle$ overlap integral. Mixing of the NN LUMO into the SQ SOMO is clearly apparent in $SOMO2_{SQNN}$ and $LUMO_{SQNN}$ (Figure 7) and exemplifies the nature of the SQ → NN donor–acceptor character of the SQNN biradical. The $\langle LUMO_{NN}|SOMO_{SQ}\rangle$ overlap integral is related to the intensity (I_{CT}) of the intraligand $SOMO2_{SQNN} \rightarrow LUMO_{SQNN}$ charge-transfer band according to eq 1.

$$I_{CT} \propto \langle LUMO_{NN}|SOMO_{SQ}\rangle^2 \quad (1)$$

Therefore, the high extinction coefficient ($\epsilon \approx 13\,500$ M^{-1} cm^{-1}) for the $SOMO2_{SQNN} \rightarrow LUMO_{SQNN}$ intraligand CT band confirms the large orbital mixing between the constituent $LUMO_{NN}$ and $SOMO_{SQ}$ basis functions in SQNN, and this is consistent with the bonding picture derived from DFT calculations as well as the simple MO picture. Additionally, this $LUMO_{NN}$–$SOMO_{SQ}$ orbital mixing provides the dominant contribution to the ground state magnetic exchange (J) according to eqs 2 and 3.[50]

$$J = J_{AF} + J_F \quad (2)$$

$$J_F = k = \int \rho(1)\rho(2) r_{12}^{-1}\, d\tau \quad (3)$$

Here J_{AF} is the antiferromagnetic contribution to the measured magnetic exchange, J_F is the ferromagnetic contribution to the measured magnetic exchange, $\rho(i)$ is the overlap density for the singly occupied orbitals ($SOMO1_{SQNN}$ and $SOMO2_{SQNN}$) in biradical SQNN, and $J_F \gg |J_{AF}|$ since $\langle SOMO_{NN}|SOMO_{SQ}\rangle = 0$. The key point here is that $LUMO_{NN}$–$SOMO_{SQ}$ orbital mixing

(50) Kahn, O. *Molecular Magnetism*; VCH: New York, 1993.

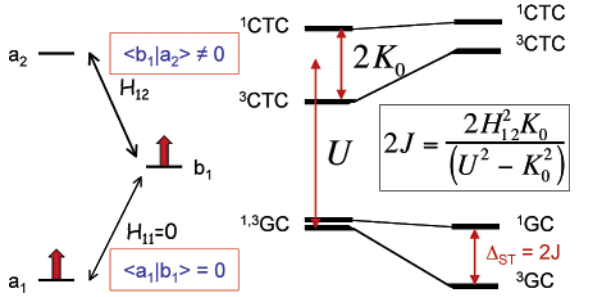

Figure 8. VBCI model. Simplified orbital diagram using $SOMO_{NN}$ (a_1), $LUMO_{NN}$ (a_2), and $SOMO_{SQ}$ (b_1) basis functions (left), and a state diagram (right) deriving from $\bar{a}_1\bar{b}_1$ (^{3}GC), $a_1\bar{b}_1$ (^{1}GC), $\bar{a}_1\bar{a}_2$ (^{3}CTC), and $a_1\bar{a}_2$ (^{1}CTC) configurations. Note that a_1, b_1, and a_2 are orbital labels and *not* Mulliken symbols, and the singlets are multideterminantal wavefunctions).

results in a large amount of $LUMO_{NN}$ orbital character being mixed into the $SOMO2_{SQNN}$ wavefunction. The $SOMO_{NN}$ function is nonbonding with respect to SQ, and therefore $SOMO1_{SQNN}$ possesses pure NN character. Thus, positive overlap density results from the NN contribution to both $SOMO1_{SQNN}$ and $SOMO2_{SQNN}$. This is an example of what is called a nondisjoint biradical.[25]

Noodleman[51,52] has described a convenient computational approach using spin-unrestricted DFT methods to evaluate the sign and magnitude of the exchange coupling, and this has been used extensively in the treatment of the exchange problem in transition metal dimers. In this method, the $S = 0$ spin state within the electronic GS is represented by a single determinant. We have used this approach to quantitatively evaluate the exchange interaction in biradical SQNN and obtain a calculated singlet–triplet gap ($2J$) for SQNN of 722 cm^{-1} with a high-spin $S = 1$ ground state. This result is in reasonable agreement with previously determined values of J derived from magnetic susceptibility ($2J > 600$ cm^{-1}) and an analysis of proton hyperfine splittings ($2J \sim 1100$ cm^{-1}).

Valence Bond Configuration Interaction (VBCI) Model. For organic biradicals, the intramolecular exchange coupling is often described within the active electron approximation, where only two magnetic orbitals are involved. An alternative description of the magnetic exchange problem in donor–acceptor biradicals is conveniently handled within the valence bond configuration interaction (VBCI) model. More importantly, the VBCI model contains parameters that can be evaluated with spectroscopic data, allowing for an evaluation of excited-state contributions to the ground state exchange. The intraligand SQ → NN charge-transfer band $Tp^{Cum,Me}M$(SQNN) is the organic analogue of metal-to-metal charge transfer (MMCT) bands observed in transition metal dimers.[30,53] One advantageous feature of these donor–acceptor biradicals is that there is only a single dominant superexchange pathway, and this leads to a straightforward determination of H_{12} ($H_{12} = H_{AB}$ in SQNN; Figure 8) within the VBCI formalism.[30] A state energy diagram for $Tp^{Cum,Me}Zn$(SQNN) constructed from electron occupation of the a_1 ($SOMO_{NN}$), b_1 ($SOMO_{SQ}$), and a_2 ($LUMO_{NN}$) basis functions is presented in Figure 8. Here, a represents the NN site, and b, the SQ site. Since the $SOMO_{NN}$ and $SOMO_{SQ}$

(51) Lovell, T.; Himo, F.; Han, W. G.; Noodleman, L. *Coord. Chem. Rev.* **2003**, *238*, 211.
(52) Noodleman, L.; Case, D. A.; Aizman, A. *J. Am. Chem. Soc.* **1988**, *110*, 1001.
(53) Creutz, C.; Newton, M. D.; Sutin, N. *J. Photochem. Photobiol., A* **1994**, *82*, 47–59.

fragments are orthogonal in this basis, the electronic coupling matrix element, H_{11}, is zero, and the singlet (^{1}GC) and triplet (^{3}GC) ground configurations are degenerate in first order. Therefore, $J_{SQNN} = 0$ within the active electron approximation, in stark contrast to the large ferromagnetic exchange determined experimentally.

According to Figure 8, the experimental observation of an intense SQ → NN CT transition necessitates a large value for H_{12}, the electronic coupling matrix element that connects $SOMO_{SQ}$ and $LUMO_{NN}$. Furthermore, the extent to which the $\bar{a}_1\bar{a}_2$ ^{3}CTC excited configuration mixes into the ^{3}GC $\bar{a}_1\bar{b}_1$ ground configuration will result in an energetic stabilization of ^{3}GC and a high-spin triplet ground state. In order to determine the magnitude of the ^{3}GC state stabilization relative to the ^{1}GC (i.e., $2J_{SQNN}$) in $Tp^{Cum,Me}$ Zn(SQNN), we use a perturbative expression (eq 4) which has been derived within this three-orbital model.

$$2J_{SQNN} = \frac{2H_{12}^2K_0}{U^2 - K_0^2} \quad (4)$$

Here, K_0 is a single-site exchange integral that splits the $a_1\bar{a}_2$ singlet and $\bar{a}_1\bar{a}_2$ triplet excited-state configurations (Hund's rule), and U is the mean charge-transfer energy, $[E(^1\text{CTC}) + E(^3\text{CTC})]/2$. This expression is similar to one derived by Girerd[35] but differs by a factor of 2. This results from the fact that eq 4 is derived for a three-state donor−acceptor system with one exchange pathway involving the excited state, as opposed to a four-state system appropriate for a symmetric dimer that possesses two equivalent exchange pathways that couple the ground and excited state. Equation 4 shows that the ferromagnetic interaction is maximized in donor−acceptor biradicals when (1) the electronic coupling matrix element that connects one monomer fragment SOMO and the other monomer fragment LUMO is maximized, (2) the single-site exchange integral is large, and (3) the intramolecular CT energy ($U - K_0$) is low. These represent key design criteria for the synthesis of donor−acceptor biradicals with high-spin ground states. Stabilization of the ^{3}GC is strongly dependent on the magnitude of the electronic coupling matrix element, H_{12}, which describes the efficiency of electron transfer from the SQ donor to the NN acceptor. Thus, a determination of H_{12} for D−A biradicals may be made from a combination of magnetic susceptibility and/or EPR measurements (J) and optical spectroscopy (U and K_0). Along these lines, Wasielewski and co-workers have recently reported an elegant method for determining H_{AB} in the weakly coupled nonadiabatic regime.[15−17,31,34,54,55] In these studies, magnetic field effects are used to experimentally determine the exchange parameter for the charge separated *excited state* biradical formed by PET. Donor−acceptor biradicals, like the ligand SQNN, are ground-state analogues of excited-state charge-separated species formed by PET. Since the exchange parameter for a biradical can be evaluated over ca. 6 orders of magnitude, H_{AB} for adiabatic and nonadiabatic cases can be probed using a variety of bridges. A major problem in determining H_{AB} in the adiabatic limit is the evaluation of K_0. This requires the observation of the spin-forbidden ^{3}GC → ^{1}CTC intraligand CT band in order to determine the ^{3}CTC−^{1}CTC splitting ($2K_0$).

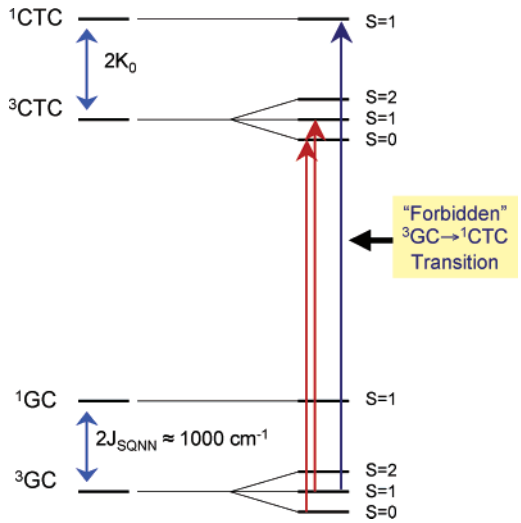

Figure 9. Energy diagram for SQNN (left) and $Tp^{Cum,Me}$Ni(SQNN) (right). Note that Ni^{II} ($S = 1$) − SQNN ($S = 1$) antiferromagnetic exchange provides a means for accessing the "forbidden" ^{1}CTC at 29 500 cm^{-1}.

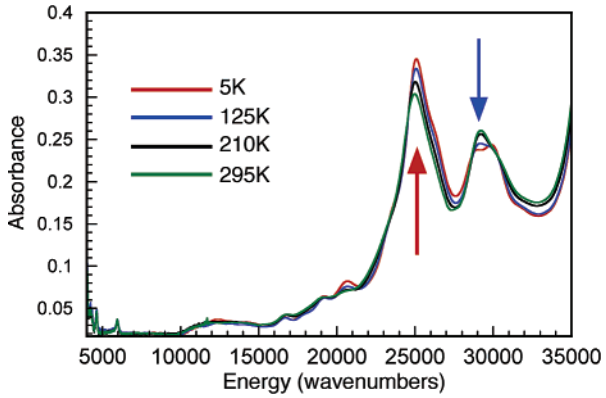

Figure 10. Variable temperature electronic absorption spectrum of $Tp^{Cum,Me}$Ni(SQNN) in a polystyrene thin film.

Analysis of Hot Bands. The incorporation of an $S = 1$ Ni(II) center in $Tp^{Cum,Me}$Ni(SQNN) leads to *antiferromagnetic* exchange between the Ni(II) ion and the $S = 1$ SQNN D−A biradical ligand.[22] This results in a diamagnetic $S = 0$ ground state with a low-lying triplet at 160 cm^{-1} ($2J_{M-SQNN}$) above the ground state singlet. Since $2J_{M-SQNN}$ is on the order of kT, variable temperature electronic absorption spectroscopy may be used to probe transitions originating from both the $S = 0$ and $S = 1$ ground state spin manifolds within the ^{3}GC of $Tp^{Cum,Me}$Ni(SQNN) (Figure 9). Therefore, at low temperatures only the $S = 0$ ground state component of the ^{3}GC is populated, and optical transitions to the $S = 1$ component of the ^{1}CTC are spin-forbidden. However, upon warming the system the $S = 1$ component of the ^{3}GC is populated allowing the observation of the formerly spin forbidden ^{3}GC → ^{1}CTC intraligand CT transition. The intensity gaining mechanism occurs through intensity borrowing from the fully spin allowed $S = 1$ ^{3}GC → $S = 1$ ^{3}CTC intraligand CT at lower energy. The 5 K electronic absorption spectrum of $Tp^{Cum,Me}$Ni(SQNN) in Figure 10 displays broad low-energy absorption features in the 10 000−15 000 cm^{-1} and 16 000−21 000 cm^{-1} regions, with additional bands centered at 25 100 cm^{-1}, 29 000 cm^{-1}, and

(54) Weiss, E. A.; Ratner, M. A.; Wasielewski, M. R. *J. Phys. Chem. A* **2003**, *107*, 3639−3647.
(55) Sinks, L. E.; Weiss, E. A.; Giaimo, J. M.; Wasielewski, M. R. *Chem. Phys. Lett.* **2005**, *404*, 244.

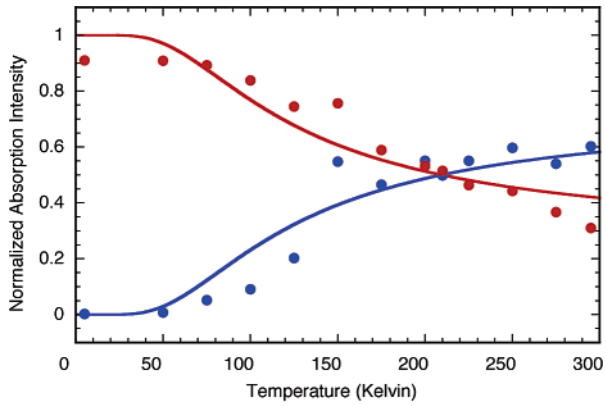

Figure 11. Normalized electronic absorption intensity changes as a function of temperature for the 25 100 cm^{-1} (red solid circles) and 29 200 cm^{-1} (blue solid circles) of $Tp^{Cum,Me}Ni(SQNN)$. The solid lines are the Boltzmann populations for the $S = 0$ (red) and $S = 1$ (blue) magnetic sublevels of Figure 10 determined from solid-state magnetic susceptibility measurements on $Tp^{Cum,Me}Ni(SQNN)$.

Scheme 2. *para*-Phenylene-Bridged Biradical $Tp^{Cum,Me}Zn(SQ-Ph-NN)$

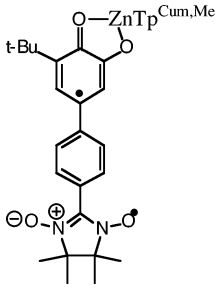

29 900 cm^{-1} similar the those observed for $Tp^{Cum,Me}Zn(SQNN)$ and $Tp^{Cum,Me}Cu(SQNN)$.

As predicted from Figure 9, when the temperature is increased a marked decrease in the 25 100 cm^{-1} band is observed with a concomitant increase in absorption intensity at 29 200 cm^{-1} (Figure 10). Collectively, this behavior is consistent with the population of the $S = 1$ magnetic component of the exchange coupled ^3GC and the appearance of the "forbidden" $S = 1$ $^3GC \rightarrow S = 1$ ^1CTC intraligand CT transition. The $^3CTC-^1CTC$ energy gap is ~4000 cm^{-1}, which is equal to $2K_0$ in the VBCI model, and U is equal to 27 000 cm^{-1}. The intensities of the 25 100 cm^{-1} and 29 200 cm^{-1} bands in $Tp^{Cum.Me}Ni(SQNN)$ can be plotted as a function of temperature, and this is displayed in Figure 11 along with the Boltzmann population of the $S = 0$ and $S = 1$ magnetic sublevels determined from magnetic susceptibility measurements on $Tp^{Cum.Me}Ni(SQNN)$.[22] The general agreement between the variable temperature electronic absorption and the magnetic susceptibility data strongly suggest that the $Tp^{Cum.Me}Ni(SQNN)$ SQ−NN ring torsion angle remains unchanged when dissolved in a polymer matrix, since this torsion is expected to affect SQNN exchange coupling.[22,56,57]

Since J, K_0, and U have now been evaluated experimentally, this allows for the magnitude of the electronic coupling matrix element to be calculated directly from eq 4 and H_{12} (i.e., H_{SQNN}) = 13 460 cm^{-1}. Under the assumption that U and K_0 are unaffected by the nature of the bridge fragment, this methodology allows for the straightforward determination of the electronic matrix element for any SQ−bridge−NN system given the magnitude of the exchange coupling, J, according to eq 5.

$$\frac{J_{SQ-Bridge-NN}}{J_{SQNN}} = \frac{H^2_{SQ-Bridge-NN}}{H^2_{SQNN}} \quad (5)$$

As an example, the magnetic exchange parameter for phenyl-bridged $Tp^{Cum.Me}Zn(SQ-Ph-NN)$ (Scheme 2)[22] has been determined to be $2J_{SQ-Ph-NN} = +200$ cm^{-1}.[22] This results in $H_{SQ-Ph-NN} = 5740$ cm^{-1} for $Tp^{Cum.Me}Zn(SQ-Ph-NN)$, which is ~56% less than the electronic coupling matrix element for $Tp^{Cum.Me}Zn(SQNN)$.

Conclusions

Donor−acceptor biradicals, like the ligand SQNN, may be viewed as ground-state analogues of excited-state charge-separated species formed by PET. As such, our work on donor−acceptor biradicals builds on the extensive PET literature relating H_{AB} to the electron-transfer rate in photoexcited D−B−A systems.[11,13,15,17,31,32,54,58−64] Since the exchange parameter for a biradical can be evaluated over ca. 6 orders of magnitude, H_{AB}'s in the adiabatic and nonadiabatic limits can be probed using a variety of bridges. In addition, the angular and distance dependence of H_{AB} can be evaluated in a straightforward manner provided a crystal structure of the donor−acceptor biradical can be determined. Furthermore, the magnitude of the electronic coupling matrix element can be related to the ground and excited-state electronic structure of the donor, bridge, and acceptor, allowing one to determine key electronic structure contributions to coherent and incoherent electron transfer/transport. Future efforts will include evaluating the effects of different bridge fragments on the electronic coupling matrix element and exploring the angular dependence of H_{AB} in various $Tp^{Cum,Me}M(SQ-Bridge-NN)$ donor−acceptor biradical complexes.

Acknowledgment. M.L.K. acknowledges the National Institutes of Health (GM-057378) and the National Science Foundation (NSF CHE-0616190) for financial assistance. D.A.S. thanks the National Science Foundation (CHE-0345263) for financial support and the Camille and Henry Dreyfus Foundation for a Camille Dreyfus Teacher-Scholar Award.

JA065384T

(56) Shultz, D. A.; Fico, R. M., Jr.; Bodnar, S. H.; Kumar, R. K.; Vostrikova, K. E.; Kampf, J. W.; Boyle, P. D. *J. Am. Chem. Soc.* **2003**, *125*, 11761−11771.
(57) Shultz, D. A.; Fico, R. M.; Lee, H.; Kampf, J. W.; Kirschbaum, K.; Pinkerton, A. A.; Boyle, P. D. *J. Am. Chem. Soc.* **2003**, *125*, 15426.
(58) He, R. X.; Duan, X. H.; Li, X. Y. *J. Phys. Chem. A* **2005**, *109*, 4154−4161.
(59) Cave, R. J.; Newton, M. D. *J. Chem. Phys.* **1997**, *106*, 9213−9226.
(60) Chambron, J. C.; Harriman, A.; Heitz, V.; Sauvage, J. P. *J. Am. Chem. Soc.* **1993**, *115*, 7419−7425.
(61) Gould, I. R.; Farid, S. *J. Phys. Chem.* **1993**, *97*, 13067−13072.
(62) Gosztola, D.; Wang, B.; Wasielewski, M. R. *J. Photochem. Photobiol., A* **1996**, *102*, 71−80.
(63) Cave, R. J.; Newton, M. D.; Kumar, K.; Zimmt, M. B. *J. Phys. Chem.* **1995**, *99*, 17501−17504.
(64) Cave, R. J.; Newton, M. D. *Chem. Phys. Lett.* **1996**, *249*, 15−19.